Lawrence Berkeley National Laboratory

Title

Ionic-surfactant-mediated electro-dewetting for digital microfluidics.

Permalink

https://escholarship.org/uc/item/4kq37633

Journal

Nature, 572(7770)

ISSN

0028-0836

Authors

Li, Jia
Ha, Noel S
Liu, Tingyi 'Leo'
et al.

Publication Date

2019-08-21

DOI

10.1038/s41586-019-1491-x

Peer reviewed

LETTER

Ionic-surfactant-mediated electro-dewetting for digital microfluidics

Jia Li[1], Noel S. Ha[2,3], Tingyi 'Leo' Liu[1,4,5], R. Michael van Dam[2,3,6,7] & Chang-Jin 'CJ' Kim[1,2,7]*

The ability to manipulate droplets on a substrate using electric signals[1]—known as digital microfluidics—is used in optical[2,3], biomedical[4,5], thermal[6] and electronic[7] applications and has led to commercially available liquid lenses[8] and diagnostics kits[9,10]. Such electrical actuation is mainly achieved by electrowetting, with droplets attracted towards and spreading on a conductive substrate in response to an applied voltage. To ensure strong and practical actuation, the substrate is covered with a dielectric layer and a hydrophobic topcoat for electrowetting-on-dielectric (EWOD)[11-13]; this increases the actuation voltage (to about 100 volts) and can compromise reliability owing to dielectric breakdown[14], electric charging[15] and biofouling[16]. Here we demonstrate droplet manipulation that uses electrical signals to induce the liquid to dewet, rather than wet, a hydrophilic conductive substrate without the need for added layers. In this electrodewetting mechanism, which is phenomenologically opposite to electrowetting, the liquid–substrate interaction is not controlled directly by electric field but instead by field-induced attachment and detachment of ionic surfactants to the substrate. We show that this actuation mechanism can perform all the basic fluidic operations of digital microfluidics using water on doped silicon wafers in air, with only ± 2.5 volts of driving voltage, a few microamperes of current and about 0.015 times the critical micelle concentration of an ionic surfactant. The system can also handle common buffers and organic solvents, promising a simple and reliable microfluidic platform for a broad range of applications.

As a hydrophobic surface is desired for a liquid-attraction mechanism to work well, we recognize that a hydrophilic surface would be preferred for a liquid-repelling mechanism. Since most materials are hydrophilic, a dewetting actuation, if found to be effective, would enable digital microfluidics just as EWOD does, but without the requirement for the hydrophobic coating. Although most electrically induced dewetting phenomena are not effective for common microfluidics because they are based on irreversible processes[17,18] or special conditions[19], studies involving surfactants have shown that reversibility may be possible. For example, electrically initiated dewetting of an aqueous film on derivatized gold electrodes has been demonstrated using redox-active surfactants[20]. Recently, by using ionic surfactants, the coefficient of a lubricated friction has been switched in a solid–liquid–solid configuration[21], and boiling bubble nucleation has been modulated in a liquid–vapour–solid system[22]. Furthermore, an organic droplet has been moved on a conjugated polymer electrode in an aqueous electrolyte[23]. However, these methods have not led to a microfluidic platform technology, which would require an electric actuation that is reversible, repeatable, strong and easily applicable to a liquid–fluid–solid system[24]. In fact, we could not obtain effective actuations with aqueous droplets containing ionic surfactants on either bare metal electrodes[21,22] or on dielectric-coated electrodes. Instead, we have discovered that a bare silicon wafer works effectively, because its native oxide is hydrophilic enough to allow easy dewetting yet thin enough

(around 2 nm) not to insulate the conductive substrate. Requiring neither the added dielectric layer nor the hydrophobic topcoat, this system may avoid the reliability problems of EWOD, while benefiting from device simplification and cost reduction.

To study the underlying principle and basic characteristics of the proposed electrodewetting mechanism, we adopted the test configuration that is usually used for electrowetting studies, as shown in Fig. 1. An elaborate setup was developed for accurate experimentation, as detailed in the Methods and Extended Data Fig. 1. The droplet contains an ionic surfactant, which consists of a charged hydrophilic 'head' group and a neutral hydrophobic 'tail' region, and is placed on an electrically conductive substrate, whose surface is highly hydrophilic. When direct-current (d.c.) voltage (or current) is applied, current flows through the conductive (or resistive) liquid and an electric field is established inside the droplet. A circuit analogy is given in the Methods and Extended Data Fig. 2. The ionic surfactant molecules migrate towards or away from the substrate under the electric field, making the drop dewet (Fig. 1a) or rewet (Fig. 1b) the surface, respectively. An exemplary result shown in Fig. 1c, d used a water droplet (pH ≈ 7) containing dodecyltrimethylammonium bromide (DTAB) on a highly doped silicon wafer, chosen for its smooth surface and native oxide. The proposed mechanism has been corroborated by three different experiments detailed in the Methods and Extended Data Fig. 3, including visualization with a fluorescent surfactant. The fluorescent intensity on two surface regions—region I (always inside droplet) and region II (outside droplet during electrodewetting but inside during wetting)— are overlaid on Fig. 1c, d. The fluorescence level is slightly higher on I.C than on I.D, supporting the illustration of Fig. 1a, b for region I. For region II, the fluorescence level on II.C is much higher than II.D, confirming that the retraction of the liquid–solid contact line by electrodewetting leaves a large amount of surfactant on the substrate immediately outside the droplet. Furthermore, the fluorescence level on II.D is as low as those on I.D and the fresh surface well outside the droplet (noted as Si), supporting the reversibility by which the adsorbed surfactant molecules are desorbed from the surface back to the droplet as the contact line advances during wetting.

All the characterization experiments were performed as described in the Methods, using aqueous droplets of three cationic surfactants and one anionic surfactant: DTAB, tetradecyltrimethylammonium bromide (TTAB), cetyltrimethylammonium bromide (CTAB) and sodium dodecyl sulphate (SDS), respectively. Observation of the ionic-surfactant-mediated dewetting may be complicated by the "autophobing" effect[25,26] caused by the surface charges. To obtain the electrodewetting effect in isolation, that is, at the isoelectric point with a negligible electric double layer and thus little autophobing effect, we used pH ≈ 2.3 (see the Methods and Supplementary Video 1) for all the characterization tests of Fig. 2, which shows only the average values for visual clarity. The complete data with error bars are presented in Extended Data Fig. 4. For surfactant concentration, Fig. 2a revealed that the four surfactants all follow a similar trend, exhibiting

[1]Mechanical and Aerospace Engineering Department, University of California, Los Angeles (UCLA), Los Angeles, CA, USA. [2]Bioengineering Department, University of California, Los Angeles (UCLA), Los Angeles, CA, USA. [3]Crump Institute for Molecular Imaging, University of California, Los Angeles (UCLA), Los Angeles, CA, USA. [4]Mechanical and Industrial Engineering Department, University of Massachusetts, Amherst, MA, USA. [5]Institute for Applied Life Sciences, University of Massachusetts, Amherst, MA, USA. [6]Department of Molecular and Medical Pharmacology, University of California, Los Angeles (UCLA), Los Angeles, CA, USA. [7]California NanoSystems Institute, University of California, Los Angeles (UCLA), Los Angeles, CA, USA. *e-mail: cjkim@ucla.edu
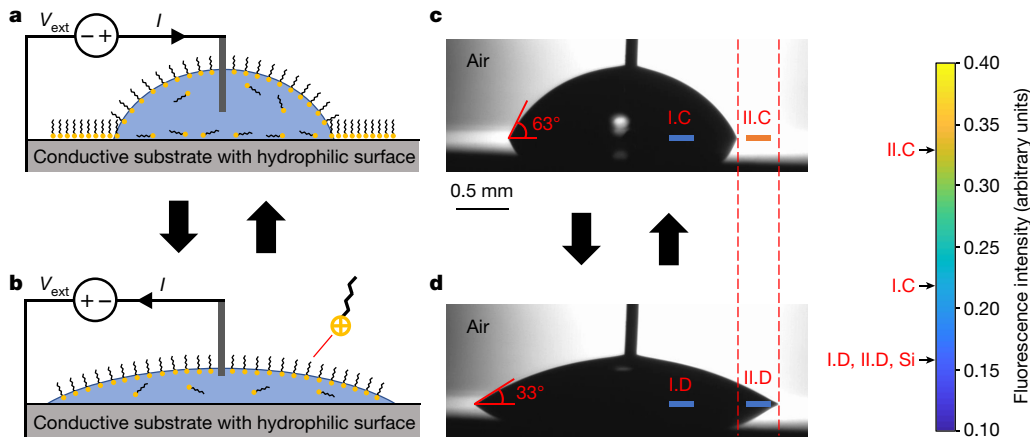
Fig. 1 | The proposed ionic-surfactant-mediated electrodewetting mechanism, studied with a sessile drop on a conductive, hydrophilic substrate. a, An electric field inside a droplet, formed by external voltage V_{ext} and current I, electrophoretically drives the ionic surfactant molecules (a cationic surfactant is shown) towards the hydrophilic substrate and deposits them on its surface (mostly near the contact line), rendering the surface hydrophobic and making the droplet dewet (that is, bead up on) the substrate. **b**, A reverse electric field formed inside a droplet removes the deposited ionic surfactant molecules from the surface and electrophoretically drives them away from the substrate, returning the surface to its hydrophilic state and making the droplet rewet (that is, spread on) the substrate. **c, d**, Electrodewetting experiment corresponding to panels a and b, respectively, with a DTAB-containing aqueous droplet (about 3 μl) on bare silicon (with native oxide) using a voltage of ±3 V with a current of ±3 μA. The surfactant concentrations on two different regions (I, II) of the substrate surface, obtained in a separate test using a fluorescent cationic surfactant, corroborate the proposed mechanism.

effective dewetting (that is, large change in contact angle and short dewetting time) in the same concentration range if the concentration is expressed with respect to critical micelle concentration (CMC). We hypothesize that when the surfactant concentration is too low, there are too few molecules to affect the surface wettability appreciably, whereas when it is too high, the contact angle is already large before actuation, leaving little room for further increase. In terms of actuation speed, Fig. 2a shows that the dewetting time was around 0.5 s, which is slower than EWOD (for example, 0.02 s)[27]. Probably this can be explained by the time needed for migration and assembly of surfactant molecules during the surfactant-mediated electrodewetting compared with the near-instantaneous polarization of the dielectric layer for EWOD. For electrical actuation, Fig. 2b shows the increase in contact angle and the corresponding current as functions of the actuation voltage for the four surfactants. The current for SDS is noticeably smaller than those for the cationic surfactants because its actuation polarity anodizes (passivates) the silicon surface. The trends found in Fig. 2 allowed us to assess other

surfactants without full characterization. A variety of (13 in total) ionic surfactants have been tested, and all of them were found to facilitate the electrodewetting, as summarized in the Methods.

With the basic characteristics of the proposed electrodewetting established, we next examine its robustness and longevity—the two most critical reliability problems of EWOD. First, the robustness is evaluated by performing electrodewetting with excessive voltages and currents. For cationic surfactants, at around 4 V and around 0.2 mA (that is, approximately 100 times above the usual 3 μA or so; see Fig. 2b), bubbles began to appear inside the droplet on both the wire and the substrate, indicating that substantial electrolysis of water was occurring. However, dewetting and rewetting continued to repeat effectively while, and even after, bubbles were generated violently at about 10 V with a runaway current above 3 mA (beyond Fig. 2b), as shown in Supplementary Video 2. This strong resilience is in contrast to EWOD, for which even slight electrolysis by leakage current would lead to a device failure.
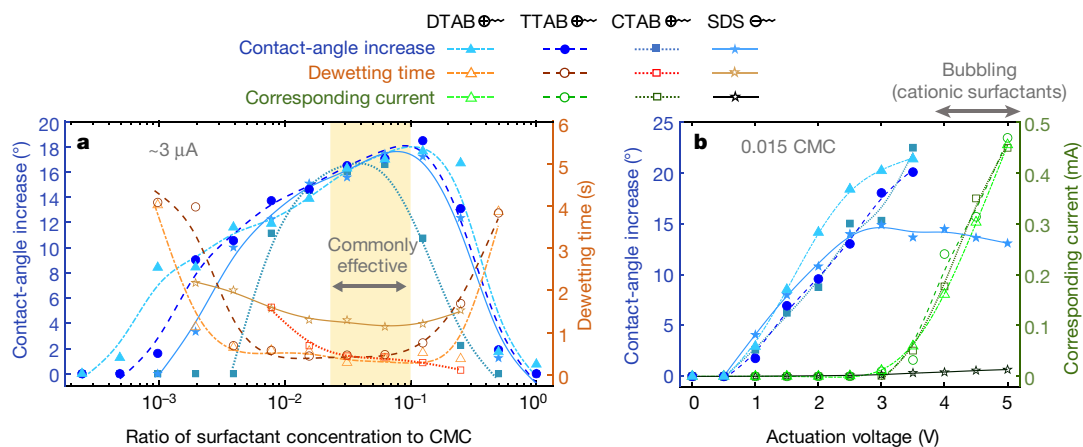

Fig. 2 | Effect of surfactant concentration and actuation voltage on the electrodewetting. a, Experiments using cationic (DTAB, TTAB, CTAB) and anionic (SDS) surfactants showed effective responses in a common range (yellow band) of concentration to CMC. The increase in contact angle was the increase from the unactuated (wetted) to the actuated (dewetted) state, where 2.5–3.0 V (corresponding to about 3 μA) was applied between the wire and substrate. The dewetting time was the time it took for the wetted state to reach the dewetted state upon actuation. **b**, Tests with the four surfactants at 0.015 CMC showed that the increase in contact angle grew with applied voltage until it reached about 3 V. For cationic surfactants, the electrolytic bubbling rendered the contact angle unmeasurable above 3.5 V. In the usual actuation range (<3.0 V), the current remains below a few microamperes for all cases.
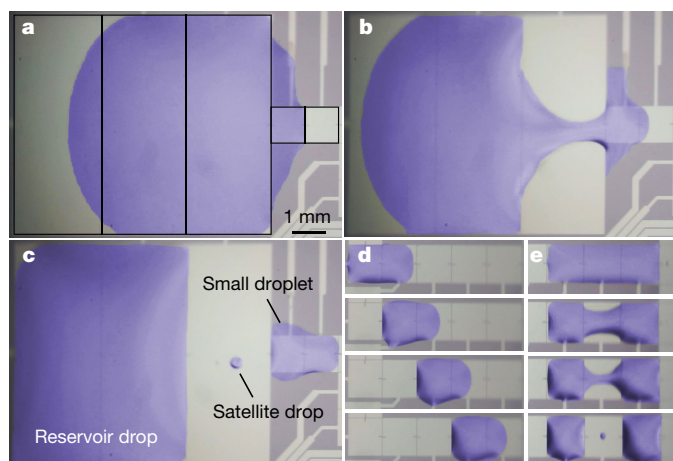
Fig. 3 | Droplet generation, transportation and splitting realized by the proposed electrodewetting. Water droplets are operated in air on a silicon device with no cover plate, using ±2.5 V (or 0 V and 5 V). Images were captured from Supplementary Video 4 and enhanced by colouring the liquid portions. **a**–**c**, Sequential images of a small (about 0.2 µl) droplet generated from a reservoir droplet (about 3 µl). **a**, The black lines were added to indicate the large electrodes underneath the reservoir. **b**, Dewetting the third reservoir electrode from left results in necking of the reservoir droplet. **c**, A droplet is generated on the two small electrodes to the right of the reservoir. **d**, **e**, Sets of four sequential images showing droplet transportation (**d**) and splitting (**e**). Along with droplet generation (panels **a** to **c**) and merging (not shown), they establish the basic operations of digital microfluidics.

Second, the longevity is evaluated by testing how long the electrodewetting actuation can proceed without degradation (for example, a decrease in the change of contact angle). By minimizing droplet evaporation (Extended Data Fig. 5), electrodewetting could be switched for over 10^4 cycles, that is, the continuous 6 h that the droplet lasted without noticeable evaporation, with no hint of deterioration, as shown in Supplementary Video 3. In comparison, dielectric charging would degrade the performance of an EWOD device after just a few hundred cycles in air. Free from the reliability problems of EWOD, the surfactant-mediated electrodewetting has thus been shown to be extremely robust and highly durable.

To assess the potential for a platform technology, we have developed a digital microfluidic device, as detailed in the Methods and Extended Data Fig. 6. Using an aqueous solution with DTAB at 0.015 CMC, we have achieved droplet generation, transportation, splitting and merging, as shown in Fig. 3 and Supplementary Video 4. Building blocks for more complex microfluidic protocols for applications[1], these key digital microfluidic operations were successfully obtained in air on an open device, that is, without the help of the frequently used filler oil and without using a cover plate. Interestingly, the droplets were transported (Fig. 3d) at a speed comparable to that in EWOD (see Supplementary Video 4) even though the observed actuation was 10–100 times slower during sessile drop tests (Fig. 2a). Although pH 2.3 was used for the demonstrations of Fig. 3 to be consistent with the characterization of Fig. 2, other pH levels can also be used. These results suggest that the proposed electrodewetting method is comparable to EWOD in performance while being inherently superior in reliability.

We now discuss the requirements of surfactant and electric current. Surfactant is rarely a concern for physical (for example, optical) applications, and the very low concentration used here (about 0.015 CMC) is acceptable even for many biochemical assays. This level is lower than the level usually found as a contaminant in environmental water (about 0.05 CMC)[28] and much lower than the level usually used in EWOD during biochemical assays, to combat fouling, for example (>1 CMC)[29]. However, ionic surfactants, especially cationic surfactants, may pose a problem to cell viability and would require additional investigation. Regarding electric current, a few microamperes per droplet is negligibly
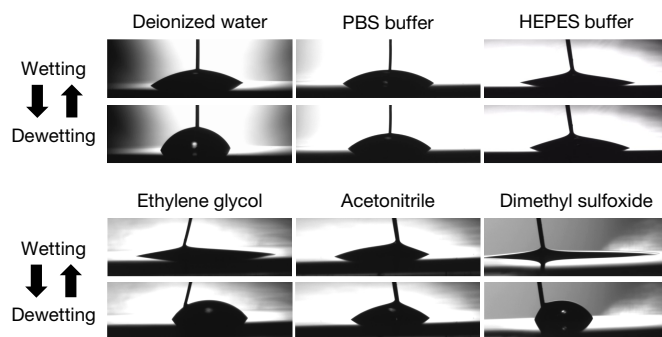

Fig. 4 | The proposed electrodewetting confirmed for a variety of liquids on bare silicon. Deionized water (Fig. 1) is included as a reference. DTAB was used for all, with different concentrations as described in the Methods. For PBS and HEPES, contact-angle changes of approximately 9° and 6° were obtained, respectively, using ±5 V. For ethylene glycol, acetonitrile and DMSO, changes of approximately 40°, 15° and 60° were obtained, respectively, using ±3 V.

small for nearly all applications. Even for life science applications, this level is much smaller than that used to monitor cell culture[30], and the associated power dissipation would be small enough for most biochemical assays.

Finally, we have explored the validity of the proposed electrodewetting for a variety of liquids: two buffer solutions widely used in biology (phosphate-buffered saline (PBS) and 4-(2-hydroxyethyl)-1-piperazineethanesulfonic acid (HEPES)); two common organic solvents used in chemistry (acetonitrile and dimethyl sulfoxide (DMSO)); and a common coolant (ethylene glycol). Although the degree of effectiveness varied, as shown in Fig. 4, the electrodewetting was found to be effective for all the liquids tested. We studied the working liquids only under the conditions in which they are typically used, in order to assess their utility, leaving more complete characterizations for future studies. The successful results with these five additional liquids suggest that the proposed electrodewetting mechanism has practical utility and versatility, opening the door for broad application.

Online content

Any methods, additional references, Nature Research reporting summaries, source data, extended data, supplementary information, acknowledgements, peer review information; details of author contributions and competing interests; and statements of data and code availability are available at https://doi.org/10.1038/s41586-019-1491-x.

1. Cho, S. K., Moon, H. & Kim, C.-J. Creating, transporting, cutting, and merging liquid droplets by electrowetting-based actuation for digital microfluidic circuits. *J. Microelectromech. Syst.* **12**, 70–80 (2003).
2. Berge, B. & Peseux, J. Variable focal lens controlled by an external voltage: an application of electrowetting. *Eur. Phys. J. E* **3**, 159–163 (2000).
3. Hayes, R. A. & Feenstra, B. J. Video-speed electronic paper based on electrowetting. *Nature* **425**, 383–385 (2003).
4. Srinivasan, V., Pamula, V. K. & Fair, R. B. An integrated digital microfluidic lab-on-a-chip for clinical diagnostics on human physiological fluids. *Lab Chip* **4**, 310–315 (2004).
5. Keng, P. Y. et al. Micro-chemical synthesis of molecular probes on an electronic microfluidic device. *Proc. Natl Acad. Sci. USA* **109**, 690–695 (2012).
6. Cheng, J.-T. & Chen, C.-L. Active thermal management of on-chip hot spots using EWOD-driven droplet microfluidics. *Exp. Fluids* **49**, 1349–1357 (2010).
7. Sen, P. & Kim, C.-J. A liquid-solid direct contact low-loss RF micro switch. *J. Microelectromech. Syst.* **18**, 990–997 (2009).
8. *Corning Varioptic Lenses* https://www.corning.com/worldwide/en/innovation/corning-emerging-innovations/corning-varioptic-lenses.html (Corning, 2019).
9. *ePlex: The True Sample-to-Answer Solution* https://www.genmarkdx.com/solutions/systems/eplex-system/?gallery=0 (GenMark Diagnostics, 2019).
10. *VolTRAX* https://nanoporetech.com/products/voltrax (Oxford Nanopore Technologies, 2019).
11. Berge, B. Electrocapillarity and wetting of insulator films by water. *CR Acad. Sci. Ser. II* **317**, 157–163 (1993).
12. Pollack, M. G., Fair, R. B. & Shenderov, A. D. Electrowetting-based actuation of liquid droplets for microfluidic applications. *Appl. Phys. Lett.* **77**, 1725 (2000).

13. Lee, J., Moon, H., Fowler, J., Schoellhammer, T. & Kim, C.-J. Electrowetting and electrowetting-on-dielectric for microscale liquid handling. *Sens. Actuat. A Phys.* **95**, 259–268 (2002).
14. Raj, B., Dhindsa, M., Smith, N. R., Laughlin, R. & Heikenfeld, J. Ion and liquid dependent dielectric failure in electrowetting systems. *Langmuir* **25**, 12387–12392 (2009).
15. Verheijen, H. J. J. & Prins, M. W. J. Reversible electrowetting and trapping of charge: model and experiments. *Langmuir* **15**, 6616–6620 (1999).
16. Latip, E. N. A. et al. Protein droplet actuation on superhydrophobic surfaces: a new approach toward anti-biofouling electrowetting systems. *RSC Adv.* **7**, 49633–49648 (2017).
17. Nave, M. I., Gu, Y., Chen-Wiegart, Y.-C. K., Wang, J. & Kornev, K. G. Is an electric field always a promoter of wetting? Electro-dewetting of metals by electrolytes probed by in situ X-ray nanotomography. *Faraday Discuss.* **199**, 101–114 (2017).
18. Hu, G.-H., Xu, A.-J., Xu, Z. & Zhou, Z.-W. Dewetting of nanometer thin films under an electric field. *Phys. Fluids* **20**, 102101 (2008).
19. Lapierre, F., Coffinier, Y., Boukherroub, R. & Thomy, V. Electro-(de)wetting on superhydrophobic surfaces. *Langmuir* **29**, 13346–13351 (2013).
20. Gallardo, B. S. et al. Electrochemical principles for active control of liquids on submillimeter scales. *Science* **283**, 57–60 (1999).
21. He, S., Meng, Y. & Tian, Y. Correlation between adsorption/desorption of surfactant and change in friction of stainless steel in aqueous solutions under different electrode potentials. *Tribol. Lett.* **41**, 485–494 (2011).
22. Cho, H. J., Mizerak, J. P. & Wang, E. N. Turning bubbles on and off during boiling using charged surfactants. *Nat. Commun.* **6**, 8599 (2015).
23. Xu, W. et al. Lateral actuation of an organic droplet on conjugated polymer electrodes via imbalanced interfacial tensions. *Soft Matter* **12**, 6902 (2016).
24. Nelson, W. C. & Kim, C.-J. Droplet actuation by electrowetting-on-dielectric (EWOD): a review. *J. Adhes. Sci. Technol.* **26**, 1747–1771 (2012).
25. Hare, E. F. & Zisman, W. A. Autophobic liquids and the properties of their adsorbed films. *J. Phys. Chem.* **59**, 335–340 (1955).
26. Mugele, F. et al. Ion adsorption-induced wetting transition in oil-water-mineral systems. *Sci. Rep.* **5**, 10519 (2015).
27. Annapragada, S. R., Dash, S., Garimella, S. V. & Murthy, J. Y. Dynamics of droplet motion under electrowetting actuation. *Langmuir* **27**, 8198–8204 (2011).
28. Sanderson, H. et al. Occurrence and weight-of-evidence risk assessment of alkyl sulfates, alkyl ethoxysulfates, and linear alkylbenzene sulfonates (LAS) in river water and sediments. *Sci. Total Environ.* **368**, 695–712 (2006).
29. Luk, V. N., Mo, G. C. H. & Wheeler, A. R. Pluronic additives: a solution to sticky problems in digital microfluidics. *Langmuir* **24**, 6382–6389 (2008).
30. Wegener, J., Keese, C. R. & Giaever, I. Electric Cell–Substrate Impedance Sensing (ECIS) as a noninvasive means to monitor the kinetics of cell spreading to artificial surfaces. *Exp. Cell Res.* **259**, 158–166 (2000).

METHODS

Electrowetting and EWOD versus ionic-surfactant-mediated electrodewetting. Able to handle small amounts of fluids, microfluidics is a key technology for many applications, such as laboratory on a chip (LOC) and point-of-care (POC) devices. Because it is difficult to miniaturize familiar continuous flow systems (consisting of pumps, tubes, valves, and so on), droplet flows are attractive for microfluidic devices. Some droplet microfluidic systems are a hybrid, transporting a stream of droplets in a carrier fluid pumped in a continuous-flow system[31], but other systems can control individual droplets using digital microfluidics[24]. Many actuation mechanisms have been shown to facilitate digital microfluidics, such as electrowetting[13] and EWOD[1,4,5,12,13], dielectrophoresis[32] and variations[33–35], surface acoustic wave[36], thermal[37] and magnetic[38] mechanisms. Among these, EWOD is the most widely used, given its ability to perform a set of basic digital microfluidics operations (create, transport, separate and merge micro- and nanolitre-sized droplets) on a simple device.

As an elegantly simple platform technology for microfluidics, electrowetting[39] (more specifically, EWOD[11–13]) has enjoyed exponential advancement during the past 15 years[24] and has culminated in multiple commercial applications[8–10]. Despite this success, however, EWOD devices are well known to suffer from reliability problems. First, since deposition of a defect-free thin film is challenging, especially across the relatively large area of some devices, the dielectric layer often experiences electric leakage or even breakdown[14], resulting in the notorious device failure by electrolysis[24]. Second, this hydrophobic topcoat, for example, polytetrafluoroethylene (PTFE), is susceptible to dielectric charging[15,40] and prone to protein fouling[16], not to mention its material and deposition costs. Despite the associated problems, the dielectric layer and hydrophobic topcoat (enabling EWOD) were the critical advances that made the once-obscure concept of electrowetting practical in applications, leading to the digital microfluidics of today.

Despite the multiple electrically induced dewetting phenomena listed in the main text, none of them appears to meet the level (in terms of reversibility, strength, simplicity and applicability) of the EWOD-based microfluidics for a liquid–fluid–solid system[24], where fluid means a gas or liquid that is immiscible with the working liquid. An electrodewetting mechanism would be effective for microfluidic applications only if the dewetting and rewetting states have a large difference in their contact angles to induce a strong actuation, the transition between the two states is reversible, and the mechanism is realized in a simple device configuration. When we attempted a surfactant-mediated electrodewetting test similar to what is described in this study with water on a gold surface, we did not observe the appreciable contact angle change found on the silicon surface. We believe gold, on which water forms a contact angle of 60°–65° (ref. 41), is not hydrophilic enough to allow effective dewetting with the surfactant. In fact, gold has been used as a hydrophobic metal for a surfactant-mediated electrowetting effect[42] and when electrowetting-on-conductor (EWOC) was explored for digital microfluidics before EWOD took off with its lowered voltages[43]. After testing many surfaces, our experience indicated that a hydrophilic surface with contact angle <25° is desirable to perform effective dewetting. This is opposite to electrowetting and EWOD, which requires a hydrophobic surface with contact angle typically >100°. Whereas the ionic-surfactant-mediated electrodewetting uses an electric field formed inside a droplet to manipulate the adsorption of ionic surfactant molecules on the solid surface, electrowetting (EWOC[44]) and EWOD use an electric field formed across the electric double layer and the dielectric layer, respectively. We note that ionic-surfactant-mediated electrodewetting is a dissipative process, unlike electrowetting, which is a conservative process in principle. Extended Data Table 1 summarizes the fundamental differences between the three mechanisms.

Contact angle measurement. The electrodewetting in this study is performed on a highly hydrophilic surface, where the contact angle of pure water is below 10°. Such a small contact angle is not only difficult to measure accurately but also sensitive to the ambient conditions. To achieve the accuracy needed and, especially, the high repeatability needed to quantitatively characterize the electrodewetting effect across different surfactants, we developed an elaborate test procedure. To show clear trends, the characterization tests (Fig. 2) involved testing over 20 different conditions for each surfactant type. The demonstration tests (Figs. 3 and 4) could be completed with many fewer conditions under less stringent controls.

The test setup for the current study is schematically shown in Extended Data Fig. 1. A platinum wire (100-μm diameter) was inserted vertically into a sessile drop on a conductive (heavily-doped p-type, resistivity <0.005 Ω·cm) silicon wafer (4-inch diameter). Two cameras, each mounted on an independent *XYZ* stage, were used to record the droplet side views, from which contact angles were obtained using ImageJ with the DropSnake plugin[45] or an in-house code to assist in measuring very low contact angles (<10°). The wafer was placed on an *XY* stage, and the wire was attached to a separate *Z* stage.

Before each test, the wire was rinsed in deionized water to remove the surfactant left from the previous test. After pipetting a droplet (about 3 μl) of surfactant solution onto a fresh wafer, we adjusted the *XY* stage to centre the droplet directly

below the wire. We then lowered the *Z* stage to insert the wire into the droplet until the tip of the wire was about 85 μm above the substrate for all tests. The orthogonal views of the droplet by the two cameras were used to assist the user in positioning the droplet and wire and later in measuring the contact angles. A source measure unit (Keithley 2425 SourceMeter) was used to apply voltage and monitor the current between the wire and substrate. All the stages were fixed on a vibration-isolation plate to obtain stable images, and all the characterization or demonstration experiments were performed in the same location in a clean room to minimize contamination of the sample surface.

The droplet profiles were recorded at 15 frames per second during all experiments. The images were extracted from the video frames and fed into an in-house code written to detect the droplet position and define the horizontal reference before measuring the contact angles for each image. Typically, the contact angles measured over 20 continuous frames were averaged to obtain the contact angle at each state. For the characterization study leading to Fig. 2, the increase in contact angle was determined from the actuated (dewetted) and recovered (passively rewetted) contact angles each obtained from 20 or more frames and the actuation (dewetting) time (speed) was determined by analysing the video recording. For each contact angle value, nine measurements were made using three new droplets on three different locations across a silicon wafer. For each dewetting time value, three measurements were made from the same recordings with some human intervention needed to define the starting point accurately.

Experiments to support the proposed mechanism (Fig. 1). The overall mechanism of the ionic-surfactant-mediated electrodewetting, illustrated in Fig. 1a, b, is that: (1) an electric field formed inside the liquid drives the ionic surfactant molecules to the substrate and helps them become deposited on its surface (Fig. 1a), and (2) a reverse electric field formed inside the liquid helps to remove the deposited ionic surfactant molecules from the surface and drive them away from the substrate (Fig. 1b). Both dewetting and rewetting consist of two phenomena: the electric migration of the surfactant molecules towards or away from the substrate and the adsorption or desorption of the surfactant molecules on and off the surface of the substrate. Here we have performed three sets of experiments to assess the electric migration, the adsorption of the surfactant and the desorption of the surfactant in the above proposed mechanism.

Circuit model. We first consider an ideal electric circuit model of the proposed electrodewetting mechanism, shown in Extended Data Fig. 2. The ionic surfactant molecules in a solution are migrated by electrophoresis under the electric field (E_l) inside the liquid formed by an external electric power source, which may provide a constant voltage (V_{ext}) (as usual) or constant current (I_{ext}) (if desired). Because the aqueous solution is electrically conductive/resistive, electric current flows through the solution to maintain the electric field necessary for the electrophoresis. In contrast to electrowetting (including EWOD), which uses a voltage but no current (at least conceptually, using d.c.), the proposed electrodewetting uses both voltage and current and can be controlled by either voltage or current. Although one can use either a voltage source (V_{ext}) or current source (I_{ext}), we usually used V_{ext} to keep the explanation consistent.

Fluorescent and regular ionic surfactant. For the experiments to assess the underlying mechanism, a fluorescent ionic surfactant was used as well as a regular ionic surfactant. Fluorescent surfactant is an attractive way to visualize the surfactant location and concentration. Among fluorescent ionic surfactants, octadecyl rhodamine B chloride (R_{18}) (ThermoFisher Scientific) was found to mediate electrodewetting. The solution was prepared by dissolving 10 mg of R_{18} in 1 ml of DMSO (Sigma Aldrich) and further diluting with deionized water to 0.2 mM. The result was an aqueous solution with about 1.5% DMSO v/v with its pH adjusted by adding concentrated hydrochloric acid. Although it showed reversible electrodewetting, a droplet containing R_{18} exhibited severe autophobing, most probably due to the presence of bulky fluorophore, which persisted even at pH 2.3, a pH value sufficient to eliminate autophobing for all the regular (non-fluorescent) cationic surfactants in this report. For the experiments that do not require fluorescence, DTAB was used as a regular ionic surfactant. A droplet of 0.2 mM DTAB solution tuned to pH 2.3 was used to avoid any autophobing effect.

Procedures. Multiple techniques were used to visualize the electrodewetting and its reversal: confocal microscopy, fluorescent microscopy, blowing droplets away and steam condensation. To acquire the fluorescent images on the substrate surface, we used an inverted fluorescent microscope (Zeiss Axio Observer Z1 with ORCA Flash 4.0 charge-coupled device (CCD) camera, 20× magnification, 2 s exposure, DsRed filter with excitation and emission wavelength at 563 nm and 581 nm, respectively).

Experiment 1 to visualize the electric migration of surfactant. The first experiment was done under a confocal microscope, using a droplet of solution containing a fluorescent surfactant R_{18}, to visualize the cationic surfactant electrophoretically driven to the surface by the electric field inside the liquid droplet when actuated. Confocal microscopy was performed with an SP8-SMD inverted confocal microscope (Leica Microsystems), using the *XZ* scan mode, 1.38 frames per second, 400

μm × 400 μm field of view, 0.992 μm optical section, around 471 nm excitation, and 625 nm (571–685 nm window) emission. Though the temporal resolution of confocal imaging (about 0.7 s) was too low to show the gradual evolution of an electrodewetting event (about 0.5 s total duration, see Fig. 2a and Extended Data Fig. 4), we could still obtain images right before and right after (separated in time by about 0.7 s) the application of the electrodewetting voltage. The two images of a vertical slice of a droplet in Extended Data Fig. 3a reveal the surfactant molecules to be originally located on or near the liquid–air interface and then populating on or near the liquid–solid interface upon actuation.

Experiment 2 to confirm the adsorption of surfactant. Experiment 1 showed that the surfactant molecules are migrated to the substrate by the electrodewetting actuation but does not necessarily confirm that the surfactant molecules are 'deposited' (adsorbed) on the surface. To assess the surfactant deposition illustrated in Fig. 1a, Experiment 2 was performed using DTAB. The surfactant adsorbed on the solid surface around and under the droplet can be maintained reasonably well after physically blowing the droplet off the surface. The blowing gas flow was roughly horizontal on the substrate from a nitrogen gun positioned about 1 cm away from the droplet centre. The level of surfactant concentration on the droplet-free surface can then be revealed by condensing steam on the surface or using fluorescent microscopy. To acquire the hydrophilicity map by steam condensation, we boiled deionized water in an electric hotpot and directed its steam over the sample surface through a plastic tube.

If the droplet is placed on a fresh silicon surface and blown away with a nitrogen gun without electrodewetting actuation, one can expect a surface essentially the same as bare silicon. When steam was directed onto this hydrophilic surface, the steam condensed everywhere, leaving only a faint pattern of where the droplet had been located, as shown in the left-hand panel of Extended Data Fig. 3b. In comparison, when the droplet was blown away while being electrodewetted, there was a clearly noticeable ring of no condensation directly outside where the electrodewetted droplet had been located, as shown in the right panel of Extended Data Fig. 3b. This ring pattern of subdued condensation visualizes the DTAB-adsorbed ring pattern. These two sets of experiments shown in Extended Data Fig. 3a, b corroborate that ionic surfactant molecules are driven to and adsorbed on the substrate surface by the proposed electrodewetting.

Experiment 3 to verify the desorption of surfactant. Experiments 1 and 2 could be performed in reverse order to assess a reverse actuation of dewetting, or rewetting. However, to strengthen support for the rewetting, which determines repeatability and real-world applicability, we performed Experiment 3 for the surfactant desorption using fluorescent ionic surfactant R_{18}, which would provide quantitative data. Unlike a sessile droplet containing a regular ionic surfactant, a sessile droplet containing the amphiphilic fatty acid R_{18} electrodewetted and recovered to wetting with poor axisymmetry and repeatability. The droplet moved around despite the inserted wire, and the contact line did not recede (dewet) and advance (rewet) around a fixed central position on the surface when repeated. Thus, in Extended Data Fig. 3c we show only three steps towards three states. The surface outside the droplet has a high concentration of surfactant (yellow) because, unfortunately, R_{18} spontaneously spreads upon droplet deposition due to autophobing, leaving a large R_{18}-covered field. In step 1, reverse (rewetting) actuation actively cleaned up much of the R_{18} molecules deposited by autophobing, bringing the droplet to a wetting state not to be influenced by the autophobing anymore (as far as the droplet does not venture out to the yellow region again). In step 2, forward (dewetting) actuation actively deposited new R_{18} molecules, bringing the droplet to a dewetting state. In step 3, reverse actuation actively cleaned up much of the R_{18} molecules deposited by electrodewetting, bringing the droplet to a wetting state. Despite the difference (that is, R_{18} has autophobing behaviour), the fluorescence intensities in Extended Data Fig. 3c indicates that the reverse actuation does clean up the surfactant molecules left outside the droplet during the preceding step, that is, surfactant deposited by either dewetting (step 2) or autophobing (before step 1) almost completely. Despite the poor reversibility with R_{18}, this three-step exercise nevertheless provides evidence that the reverse actuation removes the deposited surfactant off the surface.

The fluorescence intensities in Fig. 1c, d. By blowing the droplet away during dewetting and rewetting states and imaging the resulting dry surface with a fluorescence microscope, similarly to the above, we were able to compare the level of surfactant adsorption onto the substrate surface during the two states. The level of surfactant adsorption is expressed as the fluorescence intensity, as in the colour scale on the right side of Fig. 1. Each intensity value was calculated by averaging the intensity over a 100 μm × 100 μm area within each corresponding region. For the colour lines I.C and II.C in Fig. 1c, we applied dewetting actuation (5 V to the wire) for 10 s after rewetting actuation (−5 V to the wire) for 10 s and blew the dewetting droplet away while the dewetting actuation was on. For the colour lines I.D and II.D in Fig. 1d, we applied rewetting actuation (−5 V to the wire) for 10 s after dewetting actuation (5 V to the wire) for 10 s and blew the wetting droplet away while the rewetting actuation was on. We note that the fluorescent intensities inside

the droplet during rewetting (I.D and II.D in Fig. 1d) are practically the same as that on bare silicon, that is, free of surfactant.

The effect of surfactant concentration and actuation voltage (Fig. 2). *Preparation of silicon wafer surfaces.* For the characterization in Fig. 2, we prepared bare silicon wafer as follows: piranha clean with 3 parts of 98% sulfuric acid and 1 part of 30% hydrogen peroxide at 110 °C for over 10 min; deionized water rinse for 10 min; spin dry; bake on a hot plate at about 450 °C for 15 min to remove excess water and OH⁻ groups[46] for a consistent hydrophilicity. This process was used for all wafers including new wafers (directly out of a factory-sealed package) to ensure identical surface conditions.

Selection and preparation of surfactant solutions. Faced with numerous types and conditions of ionic surfactants, we chose DTAB, TTAB and CTAB, which have a bromine cationic head with one string of hydrocarbon tail, to see the effect of tail length. Once we found a commonly effective region, as shown in Fig. 2a, we added SDS, a typical anionic surfactant, to confirm the same region for the opposite ionic polarity. We prepared the surfactant stock solutions with DTAB, TTAB, CTAB and SDS at their CMC—14.6 mM, 3.6 mM, 0.92 mM and 8.2 mM, respectively[47]—by dissolving their powders (Sigma Aldrich) in deionized water at room temperature. We then diluted the stock solutions to various concentrations below the CMC. Hydrochloric acid (37 wt% in water, Cleanroom LP Grade, KMG Electronic Chemicals) and potassium hydroxide (45 wt% in water, Baker Analyzed grade, J.T. Baker) were used to tune the pH of the surfactant solutions, using a pH meter (PH-200, HM Digital). Next, we were able to explore a number of additional surfactants by testing them at just a couple of concentrations and voltages within the effective ranges of Fig. 2. In addition to DTAB, TTAB, CTAB, SDS and R18, we have tested 8 additional (2 cationic and 6 anionic) surfactants: didodecyldimethylammonium bromide (DDAB), dodecylamine hydrochloride (DACl), sodium decyl sulphate, sodium hexadecanesulfonate, dodecylbenzenesulfonic acid sodium salt (SDBS), dioctyl sulfosuccinate sodium salt (DOSS), potassium perfluorohexanesulfonate (PFHxS), and potassium perfluorooctanesulfonate (PFOS). All showed a clear electrodewetting effect, suggesting that the proposed electrodewetting would be applicable to most ionic surfactants, although more focused investigation will be required. The active rewetting approach (versus passive recovery to wetting after active dewetting) illustrated in Fig. 1 helps the user to address the uncertainties, including autophobing, by using different surfactants and varying fluid conditions.

The use of pH ≈ 2.3. The degree of observed electrodewetting may be complicated by the autophobing effect[25,26] but managed by controlling pH[26,48,49]. On the bare silica surface, increasing pH leads to deprotonation of silanol groups and increase negative surface charge. Cationic surfactants (for example, CTAB) are increasingly attracted to the surface the higher the pH, resulting in increased autophobing. To reduce autophobing to enable study of the electrodewetting effect in isolation, the pH can be lowered to pH ≈ 2. For anionic surfactants such as SDS, there can be some intrinsic adsorption due to hydrophobic interactions, but this can be minimized by increasing pH. As confirmed in the experiments shown in Supplementary Video 1, autophobing was absent at pH 2.3 for DTAB (representing cationic surfactants), and the change in contact angle at pH 2.3 was smaller than those at pH 11.2 and 6.5, where the autophobing effect exists. The use of a low-pH solution enabled us to perform the electrodewetting experiments with minimal autophobing interference.

Complete data. Only the average values with no error bars were shown in Fig. 2 for visual clarity. Each average value was obtained from nine measurements, as described in the Methods section 'Contact angle measurement'. The complete data are reproduced with error bars (or all data for the dewetting time) in the four separate graphs, each representing one of the four surfactant types, in Extended Data Fig. 4.

Minimizing the droplet evaporation to perform the longevity test (Supplementary Video 3). Sessile droplets of aqueous solutions commonly studied for microfluidics research, including this study, evaporate away in a few minutes, thus preventing studies of prolonged electrodewetting operation. To extend the droplet lifetime and eliminate this limitation, we developed the test setup illustrated in Extended Data Fig. 5.

Electrodewetting device demonstrating digital microfluidics (Fig. 3). *Device fabrication.* The demonstration device shown in Fig. 3 and Supplementary Video 4 was fabricated as shown in Extended Data Fig. 6. Although various other fabrication methods can be used, the current example shows a much simpler process flow compared with EWOD devices. For the current study, we started with a silicon-on-insulator (SOI) wafer of a 2.5-μm-thick top silicon layer (heavily-doped n-type, < 0.0025 Ω·cm) and 2.2-μm-thick embedded silicon dioxide on an approximately 500-μm-thick base silicon wafer (lightly-doped n-type, 5,000–10,000 Ω·cm). First, the top silicon layer was thinned down to about 1 μm (ranging 0.3–1.3 μm across the 4-inch-diameter wafer) by multiple cycles of thermal oxidation and etching of the silicon dioxide with buffered-oxide etch (BOE). This thinning would have been unnecessary if SOI wafers with desired device layer thickness were available at the time of study. The silicon electrodes were defined with a

10-μm gap between them by patterning the top silicon layer using deep reactive-ion etching with AZ5214 photoresist as the etching mask. After removing the photoresist, we put the wafer through the process described in the Methods sub-section 'Preparation of silicon wafer surfaces'.

Device operation. The silicon electrodes on the device are individually addressable and independently programmed to toggle between the electrodewetting and active rewetting voltages. To manipulate a liquid, each droplet must cover a set of at least two electrodes at two different voltage levels. Assuming a cationic surfactant and actuation with 5 V on one electrode and 0 V on the other electrode (equivalently to $+2.5$ V and -2.5 V between the droplet and substrate; see Extended Data Fig. 7), the electric field originates from the high potential electrode, passes through the droplet, and ends at the lower potential electrode. The cationic surfactants are actively desorbed from the higher potential electrode, migrated along the electric field, and actively adsorbed on the lower potential electrode, pushing the liquid from the lower potential electrode towards the higher potential electrode. An analogous situation, but with potentials reversed, would be needed to manipulate droplets containing anionic surfactants.

Relation with the wire-in-droplet configuration. To help relate the microfluidic device (Fig. 3), which is free of the electrode wire, to the wire-in-droplet setup used for studying the electrodewetting mechanism (Fig. 1), we have prepared Extended Data Fig. 7. The figure shows that the wire-free device (Fig. 3 or Extended Data Fig. 7a) is electrically equivalent to the wire–droplet system (Fig. 1 or Extended Data Fig. 7b, c) despite the difference in physical arrangement. For example, since the characterization results (Fig. 2) obtained with a wire–droplet system (Fig. 1) showed that electrodewetting works well with ±2.5 V, we operated a digital microfluidic device (Fig. 3) with d.c. power switching between 0 V and 5 V.

Feasibility tests with a variety of liquids (Fig. 4). We prepared the silicon wafer was prepared according to the Methods sub-section 'Preparation of silicon wafer surfaces'. For PBS buffer ($1\times$ Dulbecco pH 7.0–7.6) and HEPES buffer (1M Gibco by Life Technologies pH 7.2–7.5), we prepared 0.15 mM DTAB samples by diluting 15 mM DTAB (in deionized water) into 25 ml of buffer. For ethylene glycol (anhydrous, 99.8%, Sigma-Aldrich), acetonitrile (anhydrous, 99.8%, Sigma-Aldrich) and dimethyl sulfoxide (anhydrous, $\geq$ 99.9%, Sigma-Aldrich), we prepared 20 mM DTAB samples by dissolving 0.154 g DTAB powder (BioXtra, 99%, Sigma Aldrich) directly into 25 ml of ethylene glycol or solvent.

Droplets 3 μl in volume were used for each test in a normal laboratory environment. Although the individual contact-angle values may be affected (that is, they may vary over time) by the environmental variations in a normal laboratory, the changes in contact angle caused by electrodewetting at a given moment were found to be quite reproducible, suggesting robustness of the proposed mechanism for applications. Even with the limitations of the current study, we have already achieved changes in contact angle as large as 60° in air (for DMSO).

Data availability

Most data generated or analysed during this study are included in the published article. The rest will be available from the corresponding author on reasonable request.

Code availability

The custom-written code that detects the droplet position and defines the horizontal reference to assist measuring contact angles will be available on reasonable request. The code also allows one to measure very low contact angles ($<10°$).

31. Chokkalingam, V. et al. Probing cellular heterogeneity in cytokine-secreting immune cells using droplet-based microfluidics. *Lab Chip* **13**, 4740 (2013).
32. Jones, T. B., Gunji, M., Washizu, M. & Feldman, M. J. Dielectrophoretic liquid actuation and nanodroplet formation. *J. Appl. Phys.* **89**, 1441–1448 (2001).
33. Fan, S.-K., Hsieh, T.-H. & Lin, D.-Y. General digital microfluidic platform manipulating dielectric and conductive droplets by dielectrophoresis and electrowetting. *Lab Chip* **9**, 1236 (2009).
34. McHale, G., Brown, C. V., Newton, M. I., Wells, G. G. & Sampara, N. Dielectrowetting driven spreading of droplets. *Phys. Rev. Lett.* **107**, 186101 (2011).
35. Geng, H., Feng, J., Stabryla, L. M. & Cho, S. K. Dielectrowetting manipulation for digital microfluidics: creating, transporting, splitting, and merging of droplets. *Lab Chip* **17**, 1060–1068 (2017).
36. Reboud, J. et al. Shaping acoustic fields as a toolset for microfluidic manipulations in diagnostic technologies. *Proc. Natl Acad. Sci. USA* **109**, 15162–15167 (2012).
37. Davanlou, A. & Kumar, R. Thermally induced collision of droplets in an immiscible outer fluid. *Sci. Rep.* **5**, 9531 (2015).
38. Zhang, Y. & Nguyen, N.-T. Magnetic digital microfluidics—a review. *Lab Chip* **17**, 994–1008 (2017).
39. Beni, G. & Hackwood, S. Electro-wetting displays. *Appl. Phys. Lett.* **38**, 207–209 (1981).
40. Koo, B. & Kim, C.-J. Evaluation of repeated electrowetting on three different fluoropolymer top coatings. *J. Micromech. Microeng.* **23**, 067002 (2013).
41. Erb, R. A. Wettability of gold. *J. Phys. Chem.* **72**, 2412–2417 (1968).
42. Abbott, N. L., Gorman, C. B. & Whitesides, G. M. Active control of wetting using applied electrical potentials and self-assembled monolayers. *Langmuir* **11**, 16–18 (1995).
43. Moon, H., Cho, S. K., Garrell, R. L. & Kim, C.-J. Low voltage electrowetting-on-dielectric. *J. Appl. Phys.* **92**, 4080–4087 (2002).
44. Lomax, D. J. et al. Ultra-low voltage electrowetting using graphite surfaces. *Soft Matter* **12**, 8798–8804 (2016).
45. Stalder, A. F., Kulik, G., Sage, D., Barbieri, L. & Hoffmann, P. A snake-based approach to accurate determination of both contact points and contact angles. *Colloids Surf. A* **286**, 92–103 (2006).
46. Peng, L., Qisui, W., Xi, L. & Chaocan, Z. Investigation of the states of water and OH groups on the surface of silica. *Colloids Surf. A* **334**, 112–115 (2009).
47. Aguiar, J., Carpena, P., Molina-Bolívar, J. A. & Ruiz, C. On the determination of the critical micelle concentration by the pyrene 1:3 ratio method. *J. Colloid Interface Sci.* **258**, 116–122 (2003).
48. Goloub, T. P., Koopal, L. K., Bijsterbosch, B. H. & Sidorova, M. P. Adsorption of cationic surfactants on silica. Surface charge effects. *Langmuir* **12**, 3188–3194 (1996).
49. Dick, S., Fuerstenau, D. & Healy, T. Adsorption of alkylbenzene sulfonate (A.B.S.) surfactants at the alumina-water interface. *J. Colloid Interface Sci.* **37**, 595–602 (1971).
50. Ruzyllo, J. Semiconductor Glossary 2nd edn (World Scientific, 2016).

Author contributions C.-J.K. conceived the project and J.L. designed most of the work and performed all experiments. N.S.H and J.L. carried out the fluorescent experiments. T.L. and J.L. conducted the contact-angle analysis. C.-J.K., R.M.v.D. and T.L. provided overall guidance and data interpretation. C.-J.K. and J.L. prepared the manuscript and all authors contributed to it.
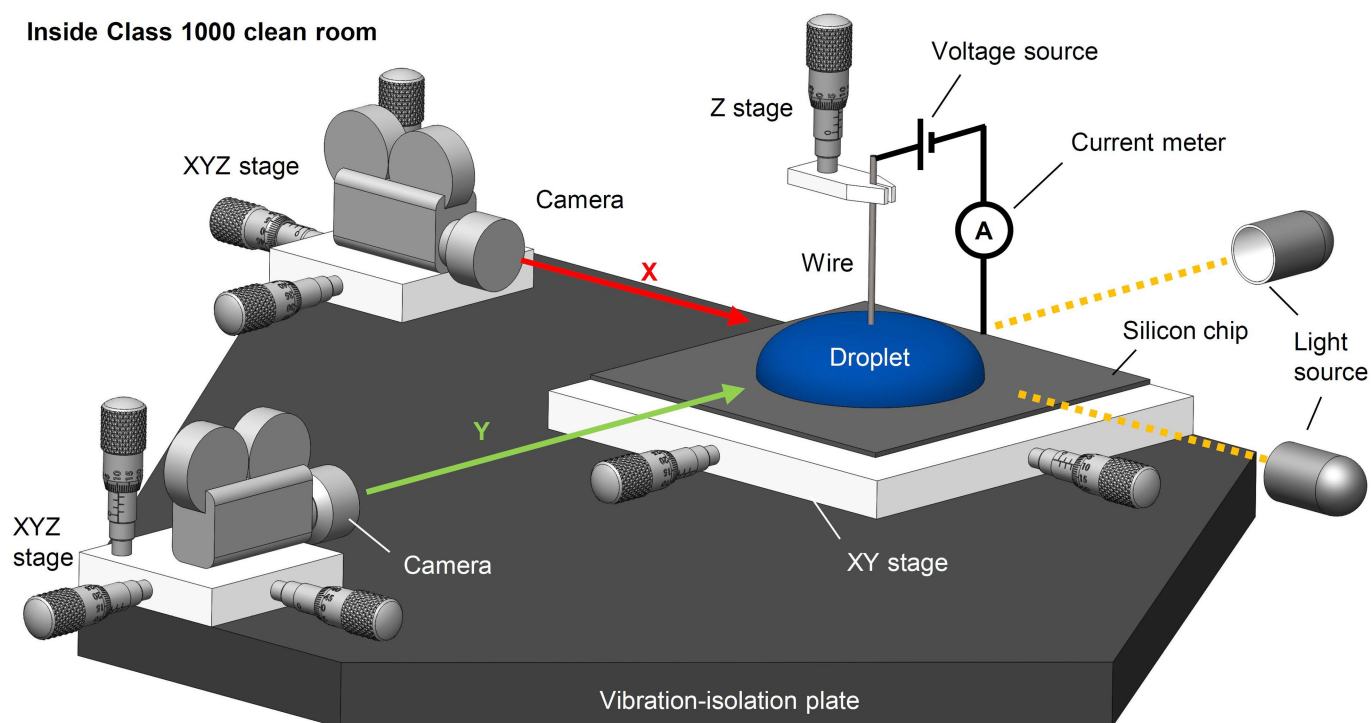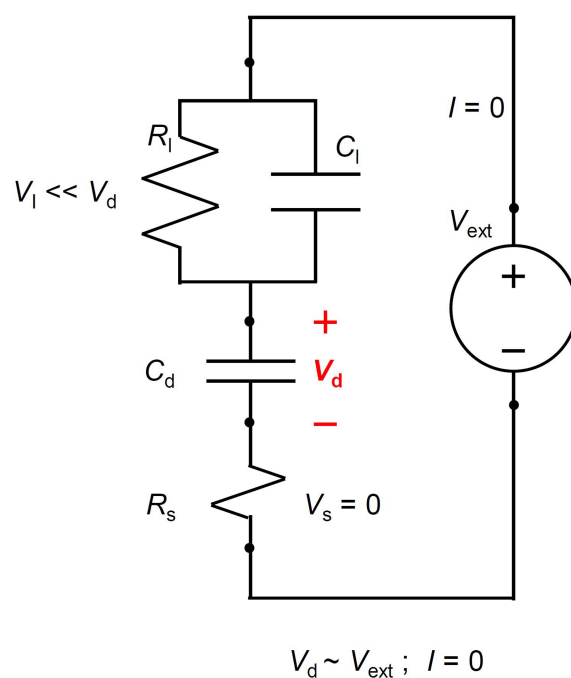
Extended Data Fig. 1 | Contact angle measurement setup with the wire–droplet system used in the current study. The silicon substrate sits on an *XY* positioning stage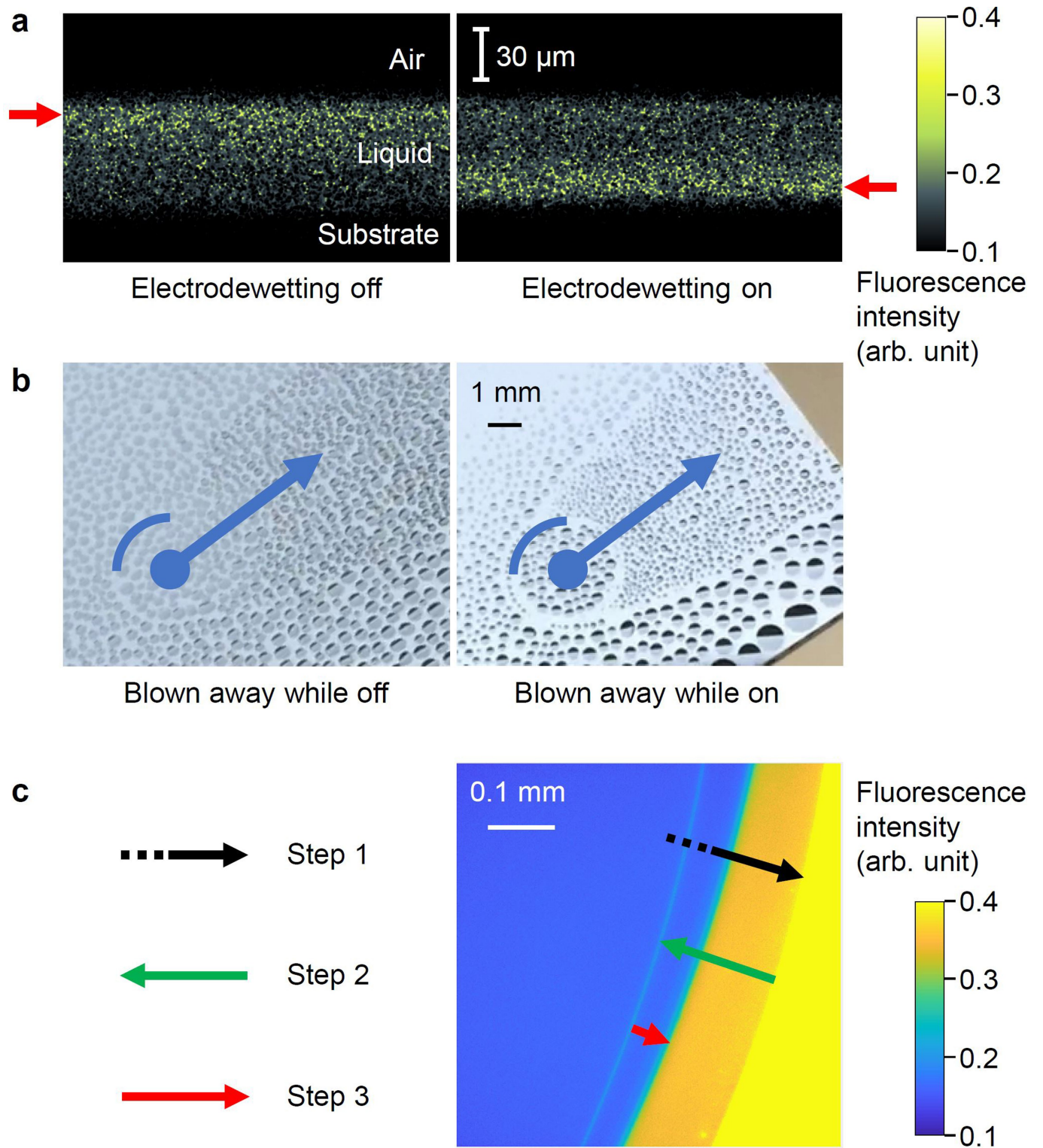; the wire electrode is attached to a *Z* positioning stage; and two cameras, each mounted on their own *XYZ* stage, view two orthogonal sides of the droplet. Not drawn to scale, for clarity. All the stages are fixed on a vibration-isolation plate.

$$V_l \sim V_{ext} \; ; \; I_l \sim V_{ext}/R_l$$

$$V_d \sim V_{ext} \; ; \; I = 0$$
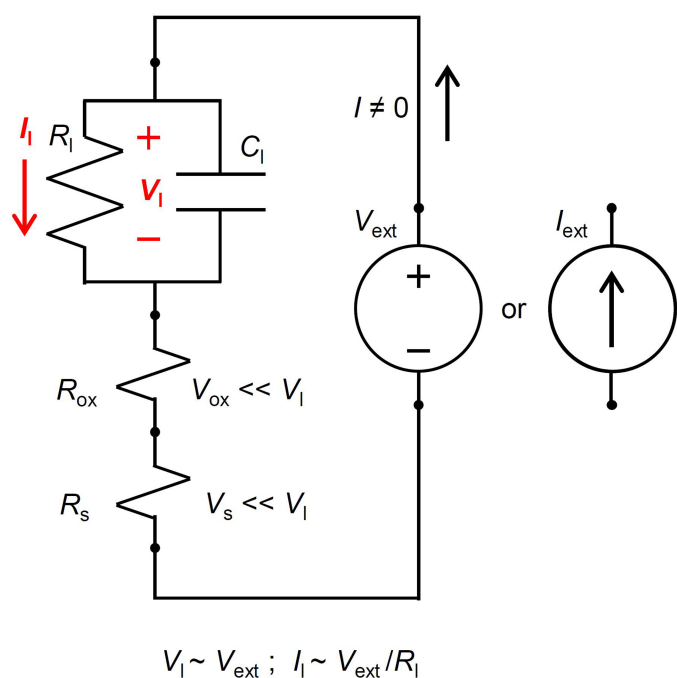
Extended Data Fig. 2 | An ideal electric circuit model of the proposed electrodewetting compared with that of the electrowetting, considering an aqueous droplet placed on a conductive substrate as seen in Fig. 1. a, For the proposed electrodewetting, a conductive substrate (R_s) is covered with a native oxide (tunnel oxide[50]), which is conductive (R_{ox}). An external electric source (V_{ext} or I_{ext}) lets the current flow through the liquid (I_l) and forms a voltage drop inside the liquid (V_l), which drives the ionic surfactant by electrophoresis. **b**, For electrowetting, a conductive substrate (R_s) is covered with an insulating dielectric material and a hydrophobic topcoat, which provide capacitance (C_d) and strong hydrophobicity. An external voltage source (V_{ext}) establishes a voltage drop across the dielectric (V_d) but little voltage drop and no current across the liquid. R_l and C_l represent the resistance and capacitance of the droplet, respectively.

a

Electrodewetting off   Electrodewetting on

Fluorescence intensity (arb. unit)

b

Blown away while off   Blown away while on

c

Step 1

Step 2

Step 3

Fluorescence intensity (arb. unit)

Surfactant cleanup by reverse electrodewetting

Extended Data Fig. 3 | See next page for caption.

Extended Data Fig. 3 | Experiments to support the proposed mechanism of electrodewetting. a, Confocal microscopic images show that a fluorescent ionic surfactant (R_{18}) is concentrated near the air–liquid interface of the droplet before actuation (red arrow), and becomes concentrated near the solid–liquid interface during the electrodewetting actuation (red arrow), corroborating that surfactant is driven to the substrate by electrodewetting. **b**, Steam condensation images reveal the wettable state of the substrate after blowing away (in the direction of the blue arrow) a water droplet containing DTAB. Unlike the unactuated droplet (left), the electrodewetted droplet leaves a dewettable area (right), corroborating that electrodewetting deposits surfactant on the surface. **c**, A water droplet with R_{18} was actuated to wet (by reverse electrodewetting), dewet (by electrodewetting), and wet (by reverse electrodewetting) the surface successively, and then the droplet was blown away to reveal a surfactant population map on the surface. Starting with an autophobed droplet, reverse electrodewetting (step 1, black arrow) cleans up the high-concentration R_{18} before electrodewetting (step 2, green arrow) deposits normal-concentration R_{18} (orange). Another reverse electrodewetting (step 3, red arrow) cleans up the normal-concentration R_{18} (orange) deposited by the previous electrodewetting, making the surface inside the droplet largely surfactant-free (blue). The fluorescence intensity on a fresh silicon substrate (that is, no surfactant) has a similar blue colour. This experiment corroborates that the deposited surfactant is removed by reverse electrodewetting actuation.
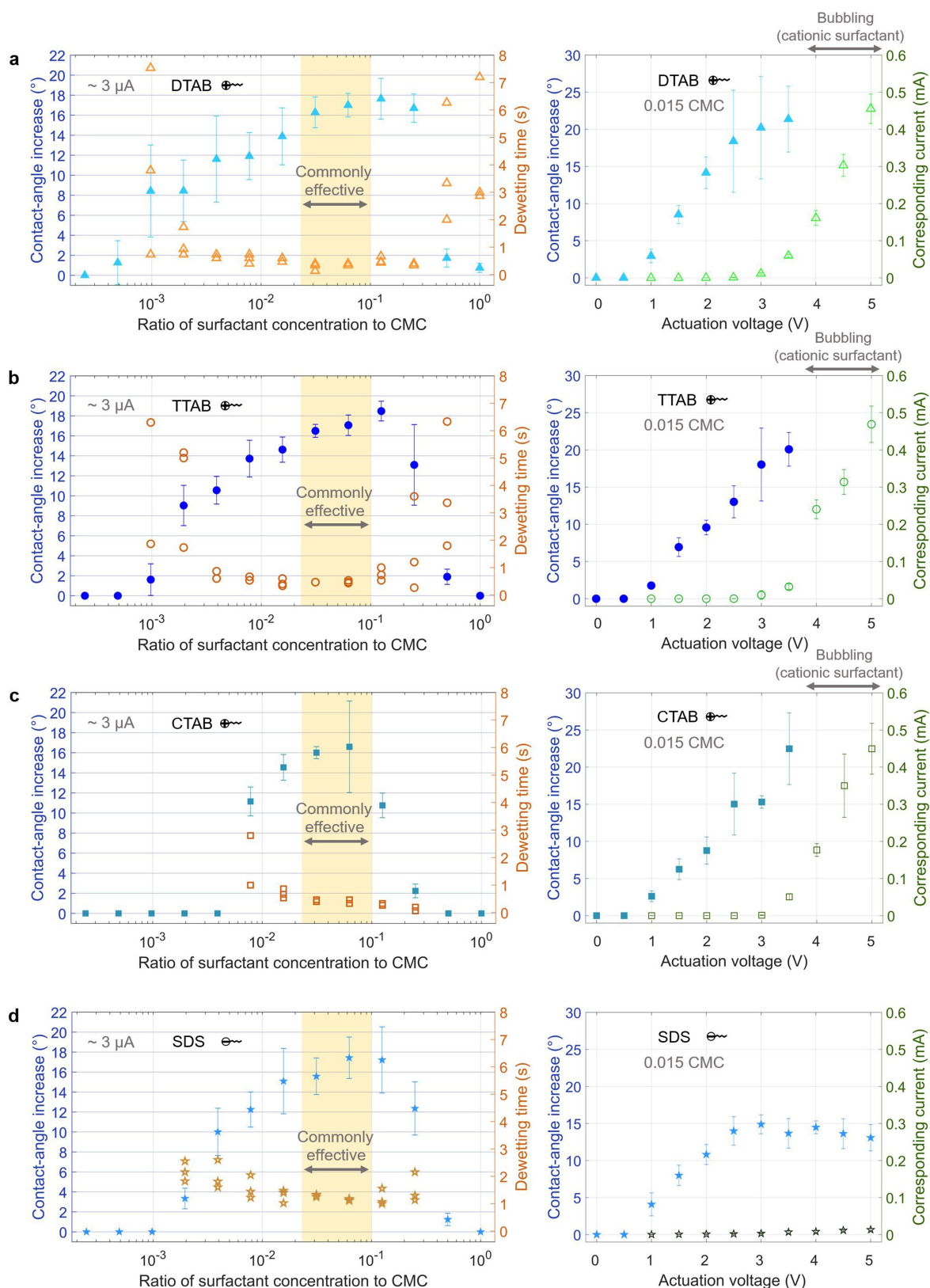
Extended Data Fig. 4 | Effect of surfactant concentration and actuation voltage (Fig. 2) shown separately for each surfactant to include error bars or all data. a-d, Contact-angle increase and dewetting time vs. surfactant concentration (left graph) and contact-angle increase and current flow vs. actuation voltage (right graph) for DTAB, TTAB, CTAB and SDS, respectively. Each symbol and error bar show an average and standard deviation of nine measurements (using about 180 images) made

with three new droplets at three different locations across a wafer. Under the natural (unactuated) state, the contact angle was found to increase with surfactant concentration for all four surfactants. However, under the electrodewetted state, the contact angle was found to increase with surfactant concentration at low concentrations and decrease at high concentrations, with a maximal value in between.
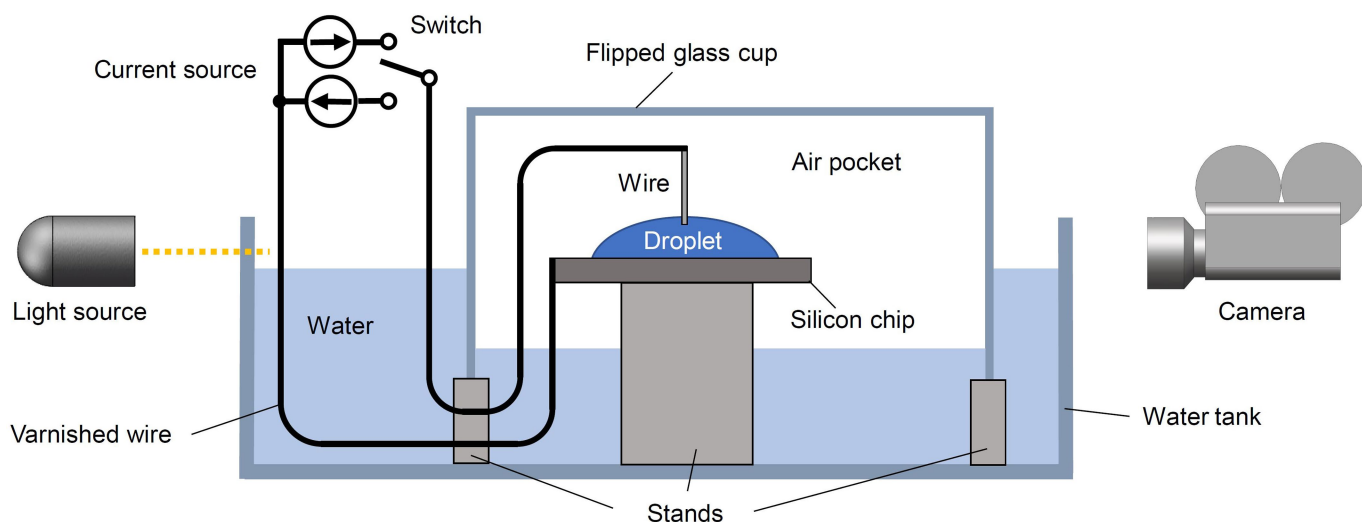
Extended Data Fig. 5 | Droplet evaporation prevention setup. A glass cup was flipped upside down into a water tank to create an air pocket containing a wire, a silicon wafer and a droplet. Two varnished wires were passed through the water to connect the wire and wafer to a power source placed outside the water tank. A relay served as a switch to toggle the polarity of the current source. The silicon wafer and glass cup were mounted on stands and the water was adjusted to be higher outside the air pocket than inside. This setup slowed down the evaporation effectively, extending the droplet evaporation time, and thus the maximum testing time, from only a few minutes to 6 h, while allowing the replacement of the silicon chip and test droplet to be quick and easy.

n++ top Si layer   Buried SiO₂   n⁻ base Si wafer

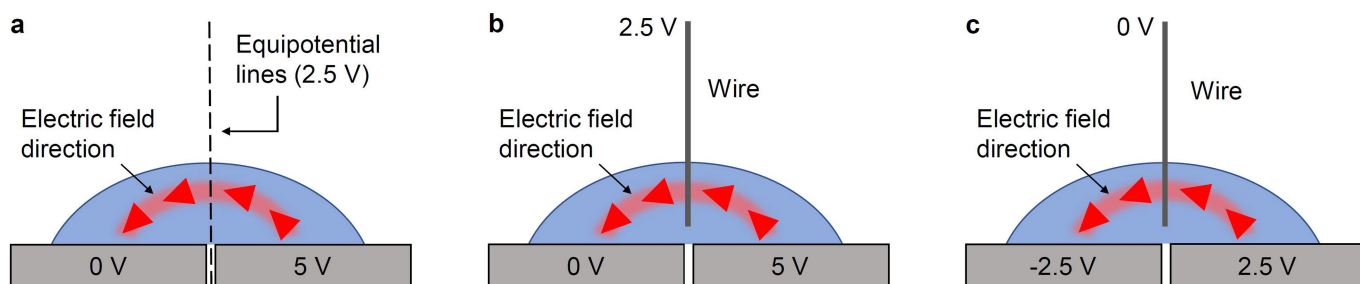1. SOI wafer with 2.5 µm highly-doped top Si and 2.2 µm buried SiO₂ on lightly-doped Si wafer.

2. Thin down top silicon to ~1 µm by multiple cycles of thermal oxidation and BOE etching.

3. Pattern top silicon layer.

Extended Data Fig. 6 | Fabrication process of the ionic-surfactant-mediated electrodewetting device used to demonstrate the digital microfluidic operations (Fig. 3). Not drawn to scale. The thin-down step was added only because SOI wafer with thin-enough top silicon layer was not available at the time of fabrication.

a

Equipotential
lines (2.5 V)

Electric field
direction

0 V | 5 V

b

2.5 V

Wire

Electric field
direction

0 V | 5 V

c

0 V

Wire

Electric field
direction

-2.5 V | 2.5 V

Extended Data Fig. 7 | Electric actuation of a droplet atop two adjacent electrodes explained with an imaginary top wire, assuming a cationic surfactant. a, When a droplet is actuated on the electrodewetting microfluidic device (Supplementary Video 4), it sits across a 0 V electrode and a 5 V electrode. For simplicity, we assume the droplet is symmetric and imagine an equipotential line of 2.5 V at the centre of the droplet. **b**, The case of a is electrically equivalent to having a 2.5 V wire in the droplet along the equipotential line. **c**, The case of b is electrically equivalent to having a 0 V wire and having a −2.5 V electrode and a 2.5 V

electrode. We note that the left half of the droplet, where an electric field is formed from the wire (0 V) to the left electrode (−2.5 V), relates to Fig. 1b (that is, dewetting), and the right half of the droplet, where an electric field is formed from the right electrode (2.5 V) to the wire (0), relates to Fig. 1a (that is, wetting). Combining the left half (dewetting) and right half (wetting), the net effect is forcing the droplet to the right. We note that the red arrows indicate the overall direction of the electric field between electrodes and do not imply electric field intensity.

Extended Data Table 1 | Electrowetting, EWOD and ionic-surfactant-mediated electrodewetting

	Electrowetting on conductor (EWOC) / Original electrowetting	Electrowetting on dielectric (EWOD) / Most widely used	Ionic-surfactant-mediated electrodewetting / This work
Needed	Appreciable electric double layer (EDL)	Dielectric layer on conductive material	Ionic surfactant in working liquid
Substrate surface	Hydrophobic	Hydrophobic	Hydrophilic
Working principle	Electric field across the EDL	Electric field across the dielectric	Electric field across the liquid